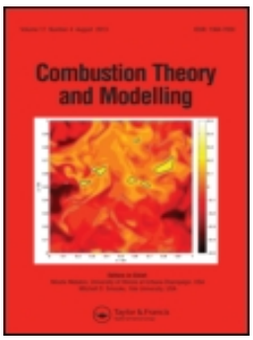

Combustion Theory and Modelling

ISSN: 1364-7830 (Print) 1741-3559 (Online) Journal homepage: https://www.tandfonline.com/loi/tctm20

Uncertainty quantification in the catalytic partial oxidation of methane

Jorge E.P. Navalho, José M.C. Pereira, Ana R. Ervilha & José C.F. Pereira

To cite this article: Jorge E.P. Navalho, José M.C. Pereira, Ana R. Ervilha & José C.F. Pereira (2013) Uncertainty quantification in the catalytic partial oxidation of methane, Combustion Theory and Modelling, 17:6, 1067-1095, DOI: 10.1080/13647830.2013.826823

To link to this article: https://doi.org/10.1080/13647830.2013.826823

Combustion Theory and Modelling, 2013
Vol. 17, No. 6, 1067–1095, http://dx.doi.org/10.1080/13647830.2013.826823

Uncertainty quantification in the catalytic partial oxidation of methane

Jorge E.P. Navalho, José M.C. Pereira, Ana R. Ervilha and José C.F. Pereira*

Universidade Técnica de Lisboa, Instituto Superior Técnico, Mechanical Engineering Department, LASEF, Av. Rovisco Pais 1, 1049-001, Lisbon, Portugal

(*Received 10 December 2012; final version received 10 July 2013*)

This work focuses on uncertainty quantification of eight random parameters required as input for 1D modelling of methane catalytic partial oxidation within a highly dense foam reactor. Parameters related to geometrical properties, reactor thermophysics and catalyst loading are taken as uncertain. A widely applied 1D heterogeneous mathematical model that accounts for proper transport and surface chemistry steps is considered for the evaluation of deterministic samples. The non-intrusive spectral projection approach based on polynomial chaos expansion is applied to determine the stochastic temperature and species profiles along the reactor axial direction as well as their ensemble mean and error bars with a confidence interval of 95%. Probability density functions of relevant variables in specific reactor sections are also analysed. A different contribution is noticed from each random input to the total uncertainty range. Porosity, specific surface area and catalyst loading appear as the major sources of uncertainty to bulk gas and surface temperature and species molar profiles. Porosity and the mean pore diameter have an important impact on the pressure drop along the whole reactor as expected. It is also concluded that any trace of uncertainty in the eight input random variables can be almost dissipated near the catalyst outlet section for a long-enough catalyst, mainly due to the approximation to thermodynamic equilibrium.

Keywords: catalytic partial oxidation; parametric uncertainty quantification; non-intrusive spectral projection; polynomial chaos; syngas

Nomenclature

English

a_V	specific surface area (m^{-1})
c_j^X	expansion mode coefficient number j of X PC expansion
C_p	specific heat under constant pressure (J kg^{-1} K^{-1})
c_v	coefficient of variation
D_p	mean pore diameter (m)
f	stochastic model solution
$F_{\text{cat/geo}}$	ratio of the catalytic surface to the total geometric surface area
f_d	deterministic model solution
$\overline{G_j G_i}$	total exchange area between volume zones j and i (m^2)
h	interphase heat transport coefficient (W m^{-2} K^{-1})
H_k	molar enthalpy of species k (J mol^{-1})
k	thermal conductivity (W m^{-1} K^{-1})
KK	total number of species

*Corresponding author. Email: jcfpereira@ist.utl.pt

$K_{\text{mat},\,k}$ interphase mass transport coefficient (m s^{-1})
N total number of uncertain parameters
N_g total number of volume zones
N_R total number of reactions
N_s total number of surface zones
P pressure (Pa)
q_R rate-of-progress variable of surface reaction R (mol m^{-2} s^{-1})
q'''_{Rad} net radiative heat flux (W m^{-3})
Re Reynolds number
S_k Selectivity of species k
Sc Schmidt number
$\overline{S_j G_i}$ total exchange area between surface zone j and volume zone i (m^2)
Sh Sherwood number
t time (s)
T temperature (K)
u interstitial flow velocity (m s^{-1})
V_k diffusion velocity of species k (m s^{-1}); volume of zone k (m^3)
W molecular weight (kg mol^{-1})
x axial reactor dimension (m)
X_k molar fraction of species k; uncertain parameter
$[X_k]$ molar concentration of gas or surface species k (mol m^{-3} or mol m^{-2})
Y_k mass fraction of species k

Greek

β extinction coefficient (m^{-1})
γ skewness
δ_w washcoat thickness (m)
ϵ porosity
κ_i absorption coefficient of volume zone i (m^{-1})
μ dynamic viscosity (kg m^{-1} s^{-1}); mean value
$\nu_{k,\,R}$ stoichiometric coefficient of species k in reaction R
$\nu'_{k,\,R}$ stoichiometric coefficient of reactant species k in reaction R
ξ random variable
ρ specific mass (kg m^{-3})
σ Stefan–Boltzmann constant (W m^{-2} K^{-4}); standard deviation
τ solid tortuosity
X_{CH_4} methane conversion
ψ_j one-dimensional orthogonal polynomial
Ψ_j multi-dimensional orthogonal polynomial
ω single scattering albedo
$\dot{\omega}_k$ molar production/consumption rate (mol m^{-2} s^{-1})

Subscripts

cat catalyst
f stochastic model solution
g gas phase; gas phase species in the bulk gas flow
g_i volume zone i
k species k; random parameter k
s solid phase; surface (adsorbed) species

s_i surface zone i
w gas phase species at the gas/wall interface

Acronyms

CI confidence interval
CPOx catalytic partial oxidation
DEA direct exchange area
FHS front heat shield
MC Monte Carlo
NISP non-intrusive spectral projection
PC polynomial chaos
PDF probability density function
ppi pore per linear inch
TEA total exchange area
UQ uncertainty quantification
UR uncertainty range

1. Introduction

The research and development of devices equipped with fuel cells to generate electric energy are being strongly encouraged for mobile and stationary applications [1]. Hydrocarbon reforming can provide a soft transition to other yet immature renewable sources of hydrogen during the development and implementation of fuel cell technology. In this context partial oxidation of hydrocarbons appears as a promising technology over other reforming strategies to produce hydrogen for small to medium scale applications [2].

Partial oxidation of gaseous hydrocarbons over catalytic surfaces, known as catalytic partial oxidation (CPOx), has received great attention due to its well recognised advantages among oxidative reforming processes. Considering methane as the fuel, the stoichiometric CPOx reaction is globally exothermic ($\Delta H_R^\circ = -36$ kJ mol^{-1}), i.e. it does not require external heat sources (as steam reforming does) and it has an H_2/CO molar ratio of two. Therefore, CPOx can be accomplished in small and simple reactors with low thermal inertia providing a good dynamic response to fast transients [2]. Ceramic materials such as cordierite or alumina are usually preferred for reactor substrates in the form of foam or extruded monoliths or even for pellets in a packed bed reactor. To increase the available catalyst surface area for reactant adsorption, the application of a washcoat layer made out of a highly porous material (onto the walls of which the catalyst particles are dispersed) is a common practice. Noble metal catalysts, such as Rh and Pt, deposited on foam monoliths proved to yield high synthesis gas selectivities and fuel conversion at millisecond contact time conditions [3, 4].

Computational modelling is currently a reliable tool for improving existing reactor designs and operating conditions. With respect to CPOx processes, several mathematical models have been proposed ranging from 1D to 3D fully distributed models, with more or less physical/transport insight and accounting for detailed multi-step surface reaction mechanisms or global kinetic mechanisms. In particular, heterogeneous 1D models with adequate chemical kinetic mechanisms and external transport correlations have proved in several studies to be appropriate in the description of temperature and mixture composition profiles along the axial reactor direction [5–8]. Uncertainty in the final solution variables will always exist to a certain extent due to the intrinsic random nature, or even to the lack of knowledge, regarding the model input parameters and also due to the model

formulation, namely in underlying assumptions, correlations, submodels, boundary conditions, etc. Uncertainty quantification (UQ) methods allow the definition of the expected solution ranges as well as solution statistics (ensemble mean, standard deviation, probability density functions, etc.) when uncertainty in input parameters or within the model formulation exists.

The classical Monte Carlo (MC) statistical methods are known to be very robust techniques, but on the other hand these methods are very computationally demanding due to the large number of solutions required to achieve accurate statistics [9, 10]. In addition, MC methods do not provide any insight on the dominant sources of parametric uncertainty [11]. For these reasons, MC methods are usually applied for validation of other statistical approaches due to the absence of any approximation or assumption on its formulation [12]. Spectral projection methods based on polynomial chaos (PC) expansion are considered more efficient for dealing with UQ than MC methods [13]. These methods can be embedded directly into the deterministic model/code through a reformulation of the governing equations (intrusive approach) or they can be used alongside the deterministic model (non-intrusive approach). The latter approach is considered to be less efficient than the former, but most often the non-intrusive approach is preferable to avoid the complex and time-consuming task associated with model reformulation of the intrusive approach [14, 15].

The non-intrusive spectral projection (NISP) approach has been widely applied in the literature to investigate parametric uncertainty. Regarding its applications in reacting flow systems, Reagan et al. [11] explored the uncertainty in thermodynamic properties and reaction rate constants for two case problems – homogeneous ignition of supercritical water oxidation and 1D premixed flame calculations; Mendes et al. [16] investigated the impact of uncertainty in porous media parameters and feed stream properties on axial temperature and CO molar fraction profiles as well as on the laminar flame speed within a fuel cell off-gas burner; Mendes et al. [17] also explored the propagation of parametric uncertainty due to uncertain model input parameters, for different operating conditions, in a 10 ppi SiC thermal partial oxidation (TPOx) reactor for synthesis gas production. Other recently published applications of the NISP approach can be found elsewhere [15, 18, 19]. Regarding intrusive spectral projection (ISP), several works have been published [14, 20, 21]. An extensive review regarding the application of polynomial chaos in UQ for CFD models can be found in [22].

The NISP approach allows the quantification of each input random variable uncertainty into the solution. The identification of the major uncertainty players in the stochastic solution is a relevant output. Consequently, a lower uncertainty range in a specific output variable can be achieved acting on the variability range (through more accurate measurements) of the dominant sources of model input uncertainty.

As far as the authors are aware, catalytic partial oxidation had not been subjected to parametric uncertainty quantification. Therefore, this paper aims to identify the main sources of uncertainty among the required model input parameters during partial oxidation of a methane–air mixture over Rh/Al_2O_3 catalyst within a highly dense foam monolith reactor. A 1D two-phase mathematical model of a fixed bed reactor accounting for proper transport and chemistry steps is considered in which the input parameters relating to geometrical properties, reactor thermophysics and catalyst loading are regarded as uncertain data. The NISP method is applied to propagate the random input data through the model and quantify its impact on the final solution.

In the next sections the deterministic model scheme and the stochastic model formulation are presented along with the identification of the main input random parameters that

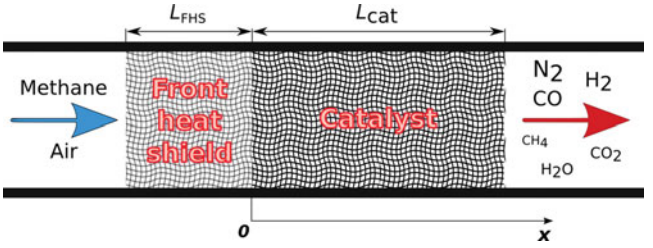

Figure 1. Schematic diagram of the physical model. $L_{FHS} = 1.0$ cm; $L_{cat} = 2.0$ cm. (colour online)

affect the stochastic model solution. This is followed by the results and ensuing discussion that precedes the final section where brief summary conclusions are presented.

2. Modelling

2.1. *Full reactor scale model: deterministic model*

The reactor is composed of two main regions, the catalytically inactive front heat shield (FHS) and the catalyst monolith, being 1.0 and 2.0 cm in length, respectively, and with an outer diameter of 1.7 cm (see Figure 1). Both reactor structures are composed by α–Al_2O_3 foams with 80 ppi. A thin Rh/α–Al_2O_3 washcoat layer ($\delta_w < 10\,\mu$m) is assumed to be deposited onto the catalyst substrate walls. A perfect linkage between both foam monoliths is considered and consequently no thermal resistance for solid conduction is taken into account.

2.1.1. *Governing equations and constitutive relations*

The mathematical model is based on a 1D two-phase model of a fixed bed reactor which accounts for a variety of phenomena:

$$\epsilon\rho_g u\frac{\partial Y_{k,g}}{\partial x} + \frac{\partial}{\partial x}\left(\epsilon\rho_g Y_{k,g}V_{k,g}\right) + a_V\rho_g K_{\mathrm{mat},k}(Y_{k,g} - Y_{k,w}) = 0 \tag{1}$$

$$\epsilon\rho_g u C_{p,g}\frac{\partial T_g}{\partial x} - \frac{\partial}{\partial x}\left(\epsilon k_g\frac{\partial T_g}{\partial x}\right) + \epsilon\rho_g\sum_{k=1}^{\mathrm{KK}_g} C_{p,k}Y_{k,g}V_{k,g}\frac{\partial T_g}{\partial x} + a_V h(T_g - T_s) = 0 \tag{2}$$

$$- a_V\rho_g K_{\mathrm{mat},k}(Y_{k,g} - Y_{k,w}) - a_V F_{\mathrm{cat/geo}}\dot{\omega}_{k,w}W_k = 0 \tag{3}$$

$$-\frac{\partial}{\partial x}\left[\tau k_s(1-\epsilon)\frac{\partial T_s}{\partial x}\right] - a_V h(T_g - T_s) + a_V F_{\mathrm{cat/geo}}\sum_{k=1}^{\mathrm{KK}_w}\dot{\omega}_{k,w}H_k + q'''_{\mathrm{Rad}} = 0. \tag{4}$$

Expressions (1) and (2) are the mass and energy balance equations of the gas phase, whereas expressions (3) and (4) are the mass and energy balance equations of the solid phase. The model takes into account diffusion and convection of heat and mass, radiative heat transfer in the solid matrix and detailed surface chemistry. Homogeneous reactions are neglected, following previous literature findings [23–25], as well as the radiative role of the reactive

gas mixture [26]. Internal diffusional limitations along the thin washcoat layer are also neglected due to its low thickness [7, 27–29].

The correction velocity formalism is considered in the mass balance equations of gas phase species to assure overall mass conservation since a non-conservative approach for the ordinary molecular diffusion is employed (mixture-averaged formalism). Thermal diffusion, relevant for low molecular weight species, is included in molecular diffusion velocities. External transport coefficients of species ($K_{\mathrm{mat},\,k}$) and heat (h) are evaluated through Sherwood and Nusselt correlations, respectively. The Sherwood correlation reported in Incera Garrido et al. [30] is employed herein (see expression (5)) and an equivalent Nusselt correlation obtained through the heat and mass transfer analogy is considered:

$$\mathrm{Sh}_k = \mathrm{Re}^{0.47} \times \mathrm{Sc}_k^{1/3} \times \left(\frac{D_p[\mathrm{m}]}{0.001} \right)^{0.58} \times \epsilon^{0.44}. \tag{5}$$

The Reynolds number (Re) in expression (5) is based on the superficial flow velocity ($u_s = u \cdot \epsilon$) and the characteristic length for the dimensionless numbers is the mean pore diameter (D_p). The perfect-gas equation of state is considered for the determination of the specific mass (ρ_g).

The surface chemistry is evaluated considering a uniform surface where the adsorbates are randomly distributed (mean-field approximation) [31]. The state of the surface is defined by its temperature and by the surface coverages of all adsorbed species. The rate-of-progress variable of each surface reaction (expression (6)) follows the mass action kinetics with the rate coefficient (k_R) given by a modified Arrhenius expression (for desorption and surface reactions) or through sticking coefficients for the adsorption reactions (see [31, 32]):

$$q_R = k_R \prod_{k=1}^{\mathrm{KK}_w + \mathrm{KK}_s} [X_k]^{\nu'_{k,R}}. \tag{6}$$

The net production or depletion rate of each adsorbed or gaseous species is evaluated through expression (7). At steady-state conditions the production rate of each surface species must be equal to its destruction rate ($\dot{\omega}_{k,s} = 0$) which results in time-independent surface species coverages. For the net production rate of gas phase species due to the heterogeneous reactions ($\dot{\omega}_{k,w}$) the summation (expression (7)) runs only over reactions that involve gas phase species (adsorption and desorption reactions):

$$\dot{\omega}_k = \sum_{R=1}^{N_R} \nu_{k,R} \times q_R. \tag{7}$$

In this work the detailed multi-step surface reaction mechanism for methane CPOx on $\mathrm{Rh/Al_2O_3}$ from the Deutschmann group [33] is employed to describe the surface chemistry. The surface site density is considered equal to 2.72×10^{-9} mol cm^{-2}. The parameter $F_{\mathrm{cat/geo}}$ presented in the source term of expressions (3) and (4) is assumed to be a scaling factor to account for an enlarged catalytic active surface area with respect to the geometric surface area (due to a washcoat deposition onto the substrate walls) [34]. This parameter takes into account the catalyst loading as well as the catalyst dispersion in the washcoat layer.

Radiative heat transfer is considered in the solid phase energy balance by the zone method [35]. The porous matrix is treated as a pseudo-homogeneous medium defined by

continuum radiative properties, such as an extinction coefficient and a single scattering albedo. Grey medium is considered as well as isotropic scattering. Since the enclosure for the radiative heat transfer analysis has a cylindrical geometry (with external boundaries dictated by the physical model – see Figure 1), in the framework of the zone method the enclosure consists of ring shaped surfaces (surface zones) coincident with the outer foam surface and cylindrical elements (volume zones) bounded by ring shaped surfaces.

According to the zone method, direct exchange areas (DEAs) which account for direct radiation between zone elements are computed through direct numerical integration. The conservation of radiative energy is verified through the summation laws of direct exchange areas [35] after the application of a smoothing technique [36]. Total exchange areas (TEAs) which consider multiple wall reflections as well as direct radiation between zone elements and scattering are evaluated through the unified matrix formulation developed by Naraghi and Chung [37] with the previously computed DEA matrices. The zone method procedure is finalised by computing the net radiative heat flux between zone elements through expression (8) to be accounted for in the solid phase energy balance equation (expression (4)):

$$q'''_{g_i} = 4\kappa_i \sigma T_{g_i}^4 - \frac{1}{V_i}\sigma \left(\sum_{j=1}^{N_s} \overline{S_j G_i} T_{s_j}^4 + \sum_{j=1}^{N_g} \overline{G_j G_i} T_{g_j}^4 \right). \tag{8}$$

The internal ring surface that surrounds both foam structures is assumed to be radiatively non-participating (through a defined zero emissivity). Radiative heat fluxes can escape towards the black inlet and outlet manifolds. The exchange temperatures for the inlet and outlet manifold surfaces are set equal to the inlet and outlet gas temperatures, respectively [38, 39].

2.1.2. *Boundary conditions*

At the inlet section of the computational domain, Danckwerts type boundary conditions are considered for the gas phase balance equations, and for the energy balance of the solid phase a radiative boundary condition is applied. At the outlet, vanishing gradients for gas phase temperature and species mass fractions are considered, and for the energy balance of the solid phase a radiative boundary condition is also applied.

2.1.3. *Numerical model*

The set of governing equations, reliable constitutive relations, underlying assumptions required for model closure and boundary conditions are implemented in an in-house version of the PREMIX code [40] from CHEMKIN software packages. A finite difference approach is considered as well as an adaptive mesh procedure. The calculation starts in an initial coarse mesh with uniformly spaced gridpoints and a modified damped Newton method is used for the iteration process. If the solution lies out of the convergence domain the program initiates a time-stepping approach in an attempt to bring the solution to the domain of convergence of the Newton method by a physically consistent evolution. The adaptive mesh procedure adds new gridpoints after the achievement of a converged solution in a given mesh location if this location does not respect the gradient and curvature resolution for each dependent variable to the degree defined by specific grid parameters.

Numerical integration of the DEAs is performed using the Gauss–Legendre quadrature with 20 Gauss points for radial and angular directions, whereas Simpson's method with five points is applied for numerical integration along the axial direction.

Table 1. Uncertainty in model input parameters.

Uncertain parameter	Mean value	Uncertainty range			References
		Limits	σ	c_v (%)	
ϵ	0.70	1 ± 0.14	0.05	7.14	[5, 7, 50]
a_V	35.00 cm^{-1}	1 ± 0.29	5 cm^{-1}	14.29	[5, 7]
D_p	0.05 cm	1 ± 0.30	0.0075 cm	15.00	[5, 7, 51]
$F_{\text{cat/geo}}$	10.00	1 ± 0.20	1.00	10.00	[27, 28]
k_s	$f(T_s)$	1 ± 0.12	0.06	6.00	[45]
τ	0.5	1 ± 0.10	0.025	5.00	[5, 47, 52]
β	20.00 cm^{-1}	1 ± 0.25	2.5 cm^{-1}	12.50	[48, 52]
ω	0.70	1 ± 0.29	0.1	14.29	[48]

Thermodynamic and transport properties are evaluated with CHEMKIN libraries [41, 42] with coefficients taken from the GRI-Mech 3.0 database [43]. The open source code CANTERA [44] is employed in this work to serve the main code as the kinetic interpreter for surface chemistry.

2.2. *Uncertain parameters*

The uncertainty in model results arises from the intrinsic random behaviour and also the lack of knowledge of properties required as model input data. These properties are mainly determined through experimental measurements and empirical correlations that are naturally marked by measurement errors and errors derived from employing fitted expressions regressed from a set of experimental data.

The most relevant model input uncertain parameters are: the geometrical properties such as porosity (ϵ), surface area to total reactor volume (a_V) and pore diameter (D_p); the ratio between catalytic and geometrical surface area ($F_{\text{cat/geo}}$); the solid conductivity (k_s); the solid tortuosity (τ); and the radiative properties of the cellular structure (β and ω). Table 1 lists the eight input physical parameters considered, their mean values and their uncertainty levels alongside the references that sustain these values. For the solid thermal conductivity, an extended range of uncertainty (by a factor of two) is adopted (see [45]).

The direct influence of the input parameters variability into the model results is straightforward when looking at the transport equations. Porosity affects advection and diffusion terms in the gas phase balance equations as well as the diffusion of heat in the energy balance equation of the solid phase; surface area to total reactor volume influences the external (interphase) transport of heat and mass and the radiative heat transport; pore diameter has an impact on external mass and heat transport through the Re number on Sh and Nu correlations; $F_{\text{cat/geo}}$ affects chemical kinetic rates; solid tortuosity and conductivity affect the diffusion of heat in the solid phase; and finally, β and ω influence the net heat flux from radiative heat exchange.

Due to the low washcoat thickness, the geometrical properties of the catalytic monolith do not differ from those of the uncoated, original foam (see [7]). Therefore, the blank FHS and the catalytic foam have equal geometrical and thermophysical properties. Radiative heat transfer properties are also set equal for both reactor structures due to the lack of relevant information.

Although empirical correlations are available to relate a_V in terms of the foam porosity and pore or strut diameter for certain foam types [30, 46], these parameters are herein

allowed to vary freely. Also for solid matrix tortuosity and radiative properties, it is well recognised that they are dependent on the geometrical properties and emissivities of the solid surfaces [47, 48]. However, these parameters are also not correlated due to the absence of information for the current ceramic foam type.

All model input uncertain parameters are described by a semicircle Beta distribution (*Beta*(3/2, 3/2)) to avoid unrealistic values that could easily appear with a Normal distribution.

2.3. *Non-intrusive spectral projection: stochastic model*

The first step of the NISP approach consists in prescribing for each random variable its mean and variability range as well as the distribution type that best characterises its uncertainty behaviour. An uncertain parameter, X, can be represented by a polynomial function of a random standard variable, ξ, in a polynomial chaos (PC) expansion, as expression (9) shows:

$$X(\xi) = \sum_{j=0}^{p} c_j^X \psi_j(\xi). \tag{9}$$

In expression (9), c_j^X are known spectral modes and $\psi_j(\xi)$ are one-dimensional orthogonal polynomials of order j ($j = 0, 1, \ldots, p$) associated with a standard random variable ξ. For each distribution type there exits an optimal class of orthogonal polynomials which minimises the required number of terms in expression (9). In the present case the random input variables are all characterised by a Beta distribution and, consequently, Jacobi polynomials are preferred.

For N independent model input uncertain parameters (X_1, X_2, …, X_N), each one being represented by expression (9) and associated with a specific random variable $\boldsymbol{\xi} = (\xi_1, \ldots, \xi_N)$, a stochastic model solution f can also be represented by a PC expansion, according to expression (10):

$$f(\boldsymbol{\xi}) = \sum_{j=0}^{P} c_j^f \Psi_j(\boldsymbol{\xi}). \tag{10}$$

In this expression c_j^f are the unknown spectral modes, $\Psi_j(\boldsymbol{\xi})$ are the multi-dimensional orthogonal polynomials and $P + 1 = N + (p)!/(N!p!)$ is the total number of terms in the PC expansion of the stochastic solution, in which p is the maximum polynomial degree of the PC expansions that represent each uncertain parameter considered (expression (9)). The unknown spectral modes or expansion mode coefficients are obtained through a Galerkin projection of the PC expansion onto the complete PC basis $\{\Psi_j\}$. Further, taking into account the orthogonality relation between polynomials and the weighting function ($W(\boldsymbol{\xi}) = \prod_{k=1}^{N} w_k(\xi_k)$), the stochastic coefficients can be determined as shown in expression (11):

$$c_j^f = \frac{\langle f_d(\boldsymbol{\xi}), \Psi_j(\boldsymbol{\xi})\rangle}{\langle \Psi_j^2(\boldsymbol{\xi})\rangle} = \frac{1}{\langle \Psi_j^2(\boldsymbol{\xi})\rangle} \int f_d(\boldsymbol{\xi})\, \Psi_j(\boldsymbol{\xi})\, W(\boldsymbol{\xi})\, \mathrm{d}\boldsymbol{\xi}. \tag{11}$$

The integral can be numerically solved by several methods (see [18, 22]), namely using a Gauss quadrature as expression (12) shows:

$$c_j^f \approx \frac{1}{\left\langle \Psi_j^2 \right\rangle} \sum_{n_1=1}^{S_1} \cdots \sum_{n_N=1}^{S_N} f_d \left[X_1 \left(\xi_1^{n_1} \right), \ldots, X_N \left(\xi_N^{n_N} \right) \right] \Psi_j \left(\xi_1^{n_1}, \ldots, \xi_N^{n_N} \right) \prod_{k=1}^{N} w_{n_k}. \quad (12)$$

Each input random variable is sampled in S_k specific collocation points given by Gauss–Jacobi quadrature because in the present work the input parameters are characterised by Beta distributions. Consequently, the total number of deterministic solutions ($f_d(\boldsymbol{\xi})$) that are required to evaluate each expansion coefficient of the stochastic model solution is given by $S_T = \prod_{k=1}^{N} S_k$. Since the Gauss quadrature rule yields exactly with S_k collocation points for a polynomial of degree up to $2S_k - 1$ and considering that the integrand in expression (11) can be seen as having degree $2p$, the minimum Gauss collocation points can be related to the PC degree by $S_k \gtrsim p + 1/2 \Rightarrow S_k \geqslant p + 1$.

In expression (12) and for the present case, $\xi_i^{n_k}$ and $w_i^{n_k}$ ($n_k = 1, \ldots, S_k$) are the Gauss–Jacobi quadrature points, which are the roots of one-dimensional orthogonal Jacobi polynomials of order S_k, and the corresponding weights, respectively.

The adopted NISP methodology is presented below with particular emphasis on the present study of uncertainty quantification.

- For each uncertain model input parameter, a specific and adequate distribution function is defined. In the present work, all uncertain parameters are parameterised through a semicircle Beta distribution. For each uncertain parameter X_k, S_k different collocation points are required ($\{X_k \left(\xi_k^{n_k} \right)\}_{n_k=1}^{S_k}$), as previously discussed, and should be computed through expression (13) considering a random variable proper for the set of orthogonal polynomials (Jacobi polynomials):

$$X_k \left(\xi_k^{n_k} \right) = \mu_k \left(L_k \xi_k^{n_k} + 1 \right), \quad n_k = 1, \ldots, S_k. \quad (13)$$

  In expression (13), μ_k and L_k are the mean and uncertainty range limits, respectively, as given in Table 1, and $\{\xi_k^{n_k}\}_{n_k=1}^{S_k}$ is the set of values of the random variable associated with a Beta probability distribution with shape parameters $\alpha = \beta = 3/2$ defined in the range $[-1.0; 1.0]$ ($\xi_k \sim Beta([-1, 1]; 3/2, 3/2)$).
- With the complete set of realisations for all input uncertain parameters $\{(X_1, \ldots, X_N)^n\}_{n=1}^{S_T}$ sampled as outlined before, deterministic model solutions are evaluated for the construction of the sample solution set.
- The multi-dimensional orthogonal polynomials, $\Psi_j(\boldsymbol{\xi})$, are evaluated from one-dimensional orthogonal polynomials, $\psi_j(\xi)$, through tensor products.
- Expansion mode coefficients of the stochastic solution PC are evaluated with expression (12) employing previously computed values.

Stochastic information as ensemble mean (μ_f), standard deviation (σ_f) and skewness (γ_f) are obtained after the above procedure is conducted with the already known solution expansion mode coefficients through the expressions (14), (15) and (16), respectively:

$$\mu_f = \langle f \rangle \quad (14)$$

$$\sigma_f = \left(\left\langle f^2 \right\rangle - \langle f \rangle^2 \right)^{1/2} \quad (15)$$

$$\gamma_f = \frac{\langle f^3 \rangle - 3\langle f \rangle \langle f^2 \rangle + 2\langle f \rangle^3}{\langle f^2 \rangle - \langle f \rangle^2} \tag{16}$$

$$\langle f \rangle = c_0^f \tag{17}$$

$$\langle f^2 \rangle = \sum_{j=0}^{P} \left(c_j^f \right)^2 \langle \Psi_j^2 \rangle \tag{18}$$

$$\langle f^3 \rangle = \sum_{j_1=0}^{P} \sum_{j_2=0}^{P} \sum_{j_3=0}^{P} c_{j_1}^f c_{j_2}^f c_{j_3}^f \langle \Psi_{j_1} \Psi_{j_2} \Psi_{j_3} \rangle . \tag{19}$$

Confidence intervals (CIs) for stochastic model solutions are computed with the corresponding cumulative distribution function numerically obtained in a post-processing stage.

3. Results

Catalytic partial oxidation at atmospheric pressure and steady-state conditions of a methane–air mixture with an air ratio of 0.31 (O/C ratio of about 1.2), a total volumetric flow rate of 10 NL min^{-1} and an inlet mixture temperature of 600 K is considered the reference operating condition for exploring uncertainty propagation through the model. Figure 2 presents the deterministic model solution for temperature (gas and solid), gaseous species (wall and bulk gas) and surface species profiles computed with the mean values for all input uncertain parameters as considered in Table 1. The predicted evolution of temperature and molar species profiles are within typical values, considering that the present mathematical model has been already extensively validated [49].

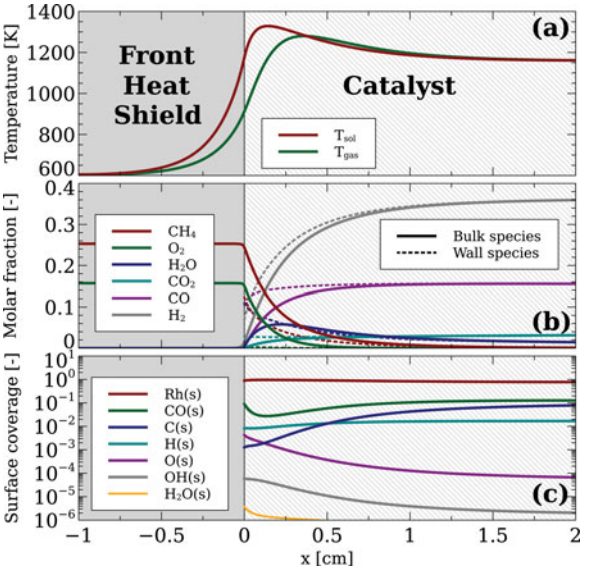

Figure 2. Deterministic model solution profiles evaluated with mean values: (a) solid and gas temperatures; (b) composition of gaseous species (bulk gas and at the bulk gas/wall interface); (c) coverages of the most abundant surface species. (colour online)

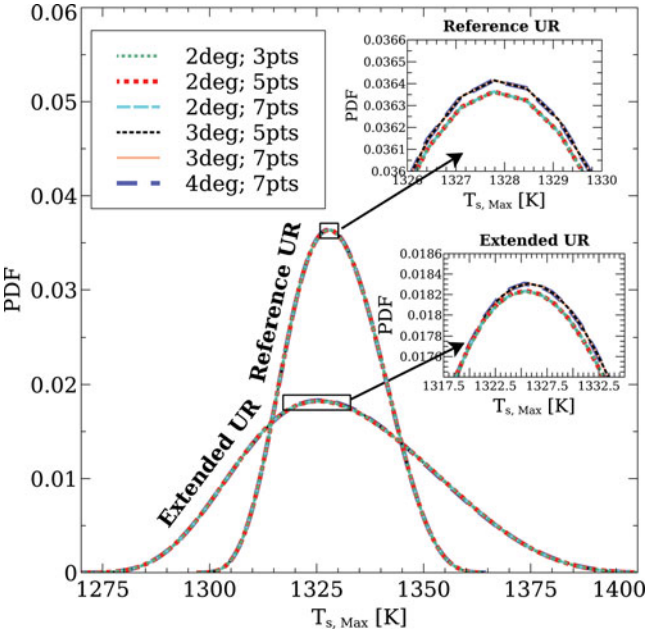

Figure 3. Stochastic convergence analysis: PDF of the maximum solid temperature. (colour online)

Two uncertainty ranges (URs) for the defined model input parameters are considered. Both ranges have the same mean values but their standard deviations are different. The reference UR considers the standard deviations defined in Table 1, whereas the extended UR takes a double value for the standard deviation of all uncertain parameters. There is an exception in the extended UR for the single scattering albedo, for which a double standard deviation would inevitably presume unphysical values and, consequently, an increase of the reference UR standard deviation by a factor of 1.5 is considered for this parameter.

The convergence of the stochastic solution using the NISP approach relies on the polynomial order (see expression (9)) and on the number of Gauss–Jacobi collocation points (see expression (12)) for each random variable. Consequently, a convergence analysis is required to infer the influence of these parameters on the stochastic solution. Figure 3 presents for both URs the convergence study carried out for the PDF of the maximum solid temperature. The polynomial degree of all random variables is varied (from second- to fourth-order) as well as the number of collocation points (from three to seven Gauss–Jacobi quadrature points). Since more than three collocation points with the eight random variables identified would require an unaffordable number of deterministic solutions (over five million with seven points, for instance) the stochastic solutions presented with more than three points are evaluated with the four major uncertainty players ($F_{\mathrm{cat/geo}}$, ϵ, a_V and k_s) as will be analysed in Figure 5(b). From Figure 3 it can be concluded for both URs that the stochastic solution is almost independent of those convergence parameters and therefore second-order polynomials with three quadrature points for each input uncertain parameter are hereafter considered.

For each UR a total of 6561 (3^8) deterministic model simulations is required to achieve the full stochastic solution (considering eight model input parameters along with the already mentioned stochastic convergence parameters). To decrease the computational time required to compute all the deterministic simulations, TEAs are evaluated in an initial

(pre-processing) stage. TEAs are functions of the extinction coefficient and scattering albedo as well as the geometry of the enclosure. Since the reactor geometry is not assumed to be uncertain, a total of nine TEA matrices (resulting from the combination of three samples for β and three samples for ω) are computed and then stored for the evaluation of net radiative heat fluxes (see expression (8)) during the processing of the whole range of deterministic runs. A total computational time of about 5.5 hours on a 2.8 GHz/8.2 GB desktop computer is required to evaluate all deterministic simulations after the computation of the TEAs. The stochastic solutions require computational times from a few seconds to several hours, depending on the number and type of outputs as well as the accuracy desired.

Figure 4(a) shows the stochastic solid temperature profiles for the ensemble mean, standard deviation and error bars with a CI of 95% for both uncertainty ranges. It shows that the reactor zones with the highest uncertain levels are observed in the FHS, a few millimetres upstream of the catalyst entrance, and downwards in the central part of the catalyst domain, and this behaviour is independent of the uncertainty range considered. In the former region values up to 150 and 75 K are observed within the upper and lower limits of the error bars for the extended and reference URs, respectively. Notice that the uncertainty in the stochastic solid temperature profiles near the inlet and outlet reactor sections tends to become almost negligible due to the absence of uncertain boundary conditions and to the low importance of the energy interphase transport term, in particular near the catalyst outlet section driven by the approximation to thermodynamic equilibrium.

The NISP method allows to quantify the effect of the prescribed uncertainty range on each random variable in the total final stochastic solution. Therefore, in Figure 4(b) the first-order and the major contributive second-order expansion mode coefficients for the reference UR can be seen. The parameters ϵ, a_V, $F_{\text{cat/geo}}$ and k_s are the dominant input uncertain sources regarding the solid temperature profile. Along the FHS, the porosity dominates the remaining parameters because of its direct impact on the heat diffusion term of the solid phase. Solid tortuosity and thermal conductivity, which also have a direct influence on the diffusive term, present a lower importance than porosity because the term $(1 - \epsilon)$ (see expression (4)) has a relative uncertainty level (c_v) of four to five times higher than τ and k_s (see Table 1). For the same reason, k_s has a higher influence on the total uncertainty than τ ($c_v(k_s) > c_v(\tau)$). In the catalyst region, a_V and $F_{\text{cat/geo}}$ are by far the most important parameters. Uncertainty in the radiative heat transfer parameters does not play an important role in the achieved solution despite the large uncertainty prescribed for these parameters (see c_v in Table 1). This is not a surprising remark since the highly dense nature of the employed 80 ppi foam assigns a negligible effect for radiative heat transport compared with solid conduction. The low values registered for the second-order coefficients compared with the first-order coefficients allow one to anticipate good stochastic convergence, which reinforces the stochastic convergence analysis presented before.

The maximum solid temperatures attained in catalytic oxidation processes are usually an important issue to be aware of during catalyst operation due to the loss of catalyst activity (catalyst deactivation) triggered by high temperatures. Figure 5(a) shows the PDF of the stochastic maximum surface temperature for both URs, their ensemble mean values as well as the 50 and 95% CIs. A different shape of these PDFs compared to the defined ones (semicircle Beta distributions) appeared due to the nonlinearities and the effective stochastic multi-dimensionality in the model scheme. The asymmetries and the tails to the right are easily seen and are confirmed by positive skewness values (γ). Differences in the maximum solid temperatures up to 45 and 75 K are noticeable within the envelopes corresponding to a CI of 95% for the reference and extended URs, respectively. Figure 5(b)

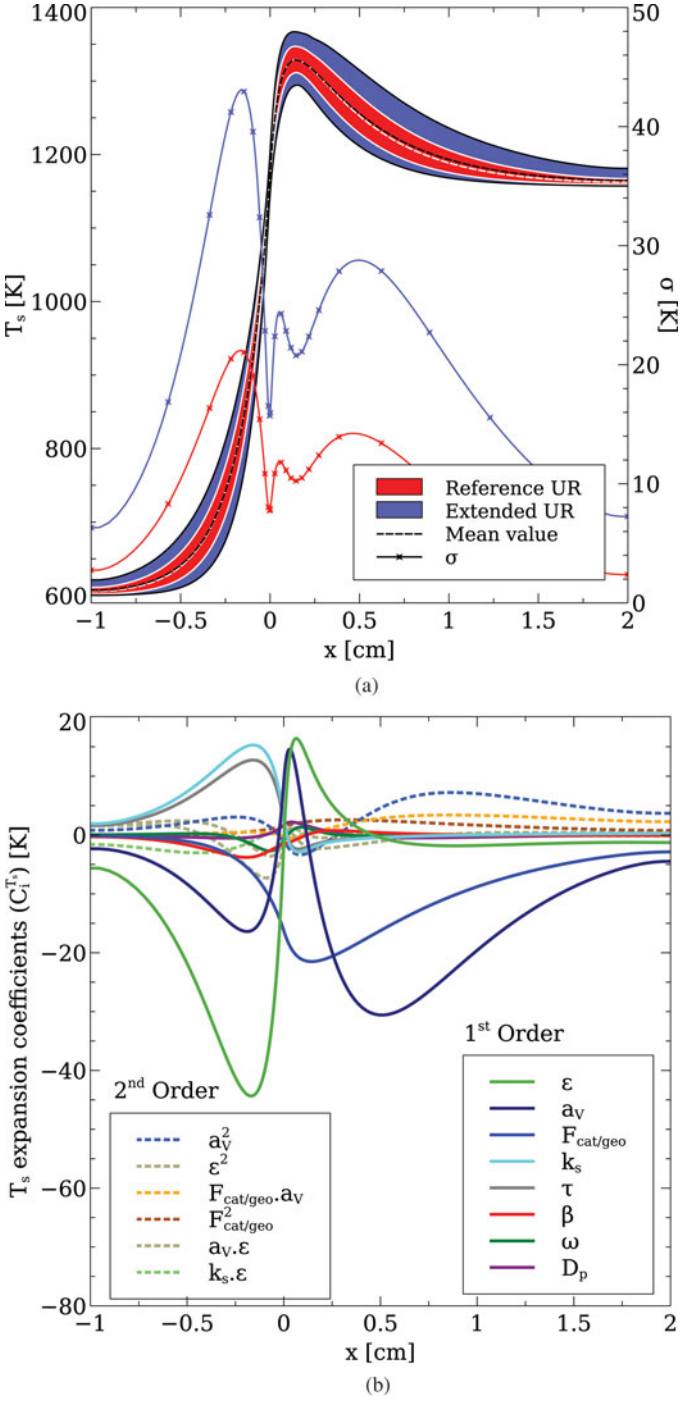

Figure 4. Stochastic solution profiles of solid temperature: (a) ensemble mean, standard deviation and error bars with 95% CI for the reference and extended URs; (b) most relevant expansion mode coefficients for the reference UR. (colour online)

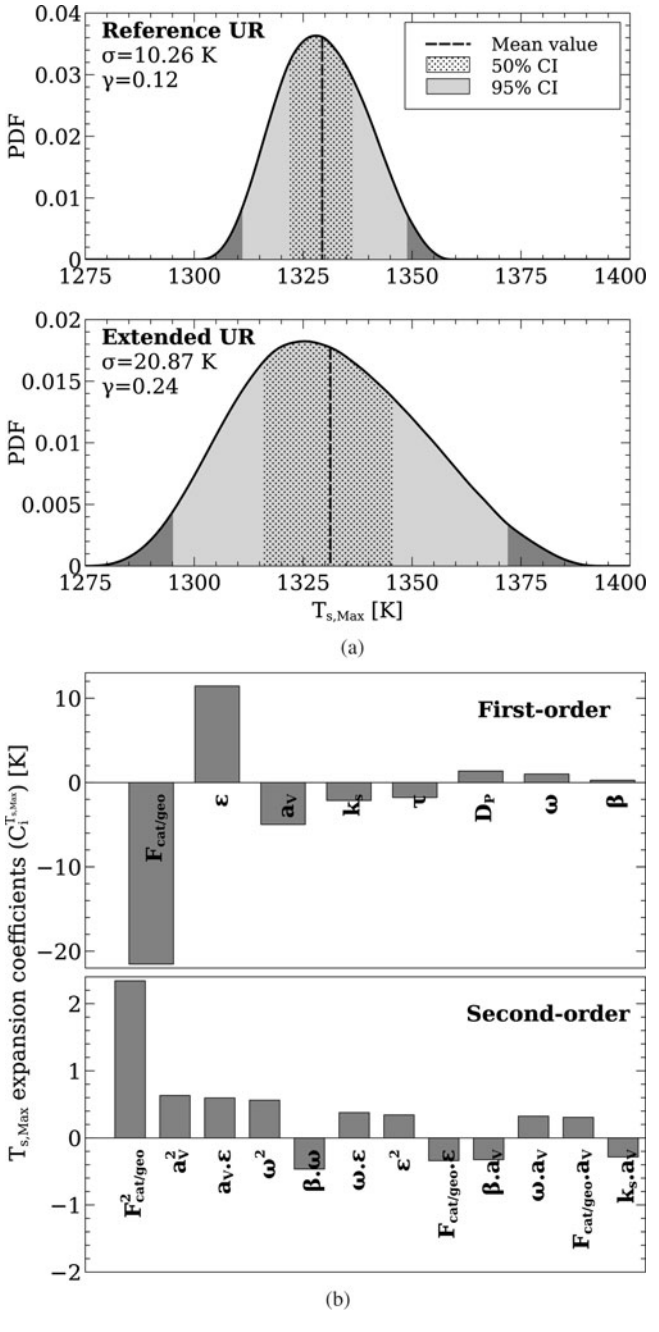

Figure 5. Stochastic solution of the maximum surface temperature: (a) PDF along with 50 and 95% CIs, ensemble mean value, standard deviation and skewness for both URs; (b) most relevant expansion mode coefficients for the reference UR. (colour online)

shows that $F_{\text{cat/geo}}$, ϵ, a_V and k_s are the main players in the stochastic maximum solid temperature, as was considered before in the stochastic convergence analysis.

Regarding gas temperature profiles, Figure 6(a) presents for both URs the stochastic mean values, standard deviations and the error bars for a CI of 95%. The uncertainty in the

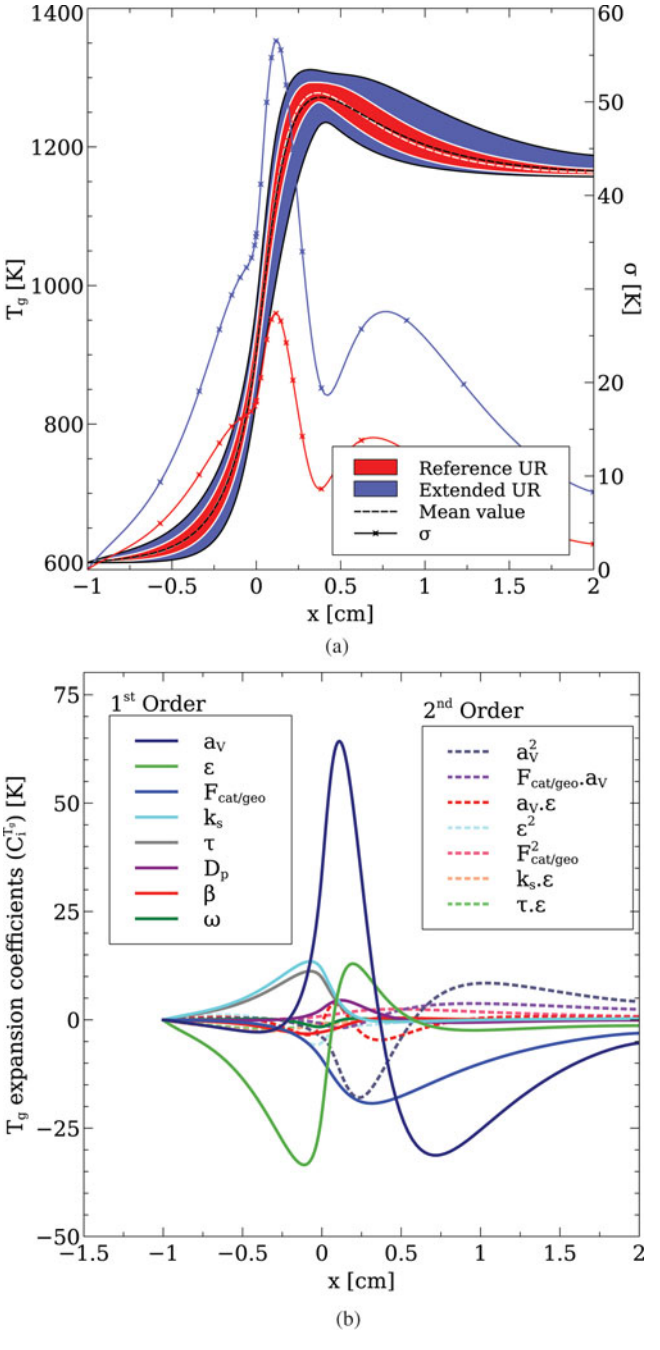

Figure 6. Stochastic solution profiles of gas temperature: (a) ensemble mean, standard deviation and error bars with 95% CI for the reference and extended URs; (b) most relevant expansion mode coefficients for the reference UR. (colour online)

gas temperature profile achieves its maximum value slightly after the catalyst inlet section. Figure 6(b) demonstrates that the specific surface area is the parameter that contributes more to this high uncertainty level because of its influence on the external heat transport term. Parameters that do not have any direct influence on the gas phase energy balance (expression (2)), such as τ, k_s, $F_{\text{cat/geo}}$, β and ω, are also responsible for the uncertainty registered in the gas temperature profiles through the external transport term. At the FHS entrance ($x = -1.0\,\text{cm}$), a negligible uncertainty is noticed and explained through the absence of relevant thermal gradients. This makes the Danckwerts boundary condition applied on the gas phase energy balance behave as a Dirichlet boundary condition. Also noticeable is the uncertainty decay as thermodynamic equilibrium is reached, i.e. in sections located farther away from the catalyst inlet section.

Figure 7 presents the stochastic solution profiles and spectral decomposition for molar fractions of two species in the bulk gas flow: methane (a representative of reactant species) and hydrogen (a representative of product species). Figures 7(a) and 7(c) reveal that upstream of the catalyst inlet section there are no uncertainties in species profiles because the mixture composition remains constant due to the absence of chemical reactions (inert walls) and molecular diffusion. In fact, advection is the only mode of mass transfer in the bulk gas along the major part of the FHS. Very near the catalyst entrance (from the upstream side – $x \lesssim 0^{-}$ cm) molecular diffusion starts to gain importance due to steep species mass gradients that establish farther downstream. The reactor axial sections where both species profiles present their maximum uncertainty level are located in the first few millimetres of the catalyst ($x < 5.0\,\text{mm}$). As the distance towards the outlet section decreases the uncertainty decreases as well. This is a common trend verified for all dependent variables (species and thermal profiles). Regarding the expansion mode coefficients (see Figures 7(b) and 7(d)) a_V, $F_{\text{cat/geo}}$ and ϵ are the most crucial parameters decreasing the extent of uncertainty in both species molar profiles.

The uncertainty levels in the axial stochastic solution profiles of temperature and bulk gas reactive species (all species except the diluting species – N_2) composition for both URs are presented in Figure 8. The coefficient of variation allows the comparison of the uncertainty range in different random variables. Therefore, along the major part of the FHS the solid temperature is more affected by the prescribed uncertainty in the input parameters than the gas temperature. No uncertainty in the reactive species composition is observed far upstream from the catalyst inlet section. In the catalyst region the uncertainty in the gas temperature dominates the solid temperature and the reactive species composition. Moreover, the level of uncertainty in the gas and solid temperatures and the reactive species composition declines towards the outlet section.

The selectivities of hydrogen and carbon monoxide are generally assumed as key parameters for monitoring the performance of the CPOx process. The hydrogen selectivity (S_{H_2}) and carbon monoxide selectivity (S_{CO}) are evaluated with the bulk gas species composition through the expressions (20) and (21), respectively:

$$S_{H_2} = \frac{X_{H_2,g}}{X_{H_2,g} + X_{H_2O,g}} \tag{20}$$

$$S_{CO} = \frac{X_{CO,g}}{X_{CO,g} + X_{CO_2,g}}. \tag{21}$$

Figure 9 shows the stochastic solution profiles for S_{H_2} and S_{CO} as well as their first-order and the main contributive second-order expansion mode coefficients. Figure 9(a) reveals

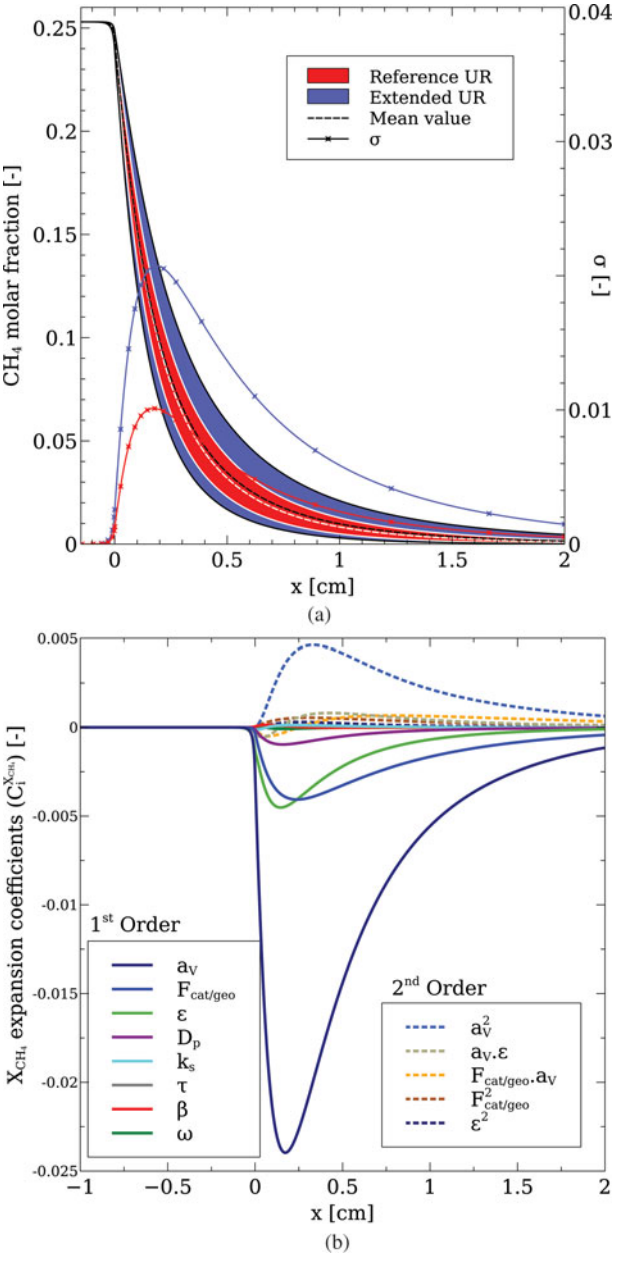

Figure 7. Stochastic solution profiles of bulk CH_4 molar fraction: (a) ensemble mean, standard deviation and error bars with 95% CI for the reference and extended URs; (b) most relevant expansion mode coefficients for the reference UR. Stochastic solution profiles of bulk H_2 molar fraction: (c) ensemble mean, standard deviation and error bars with 95% CI for the reference and extended URs; (d) most relevant expansion mode coefficients for the reference UR. (colour online)

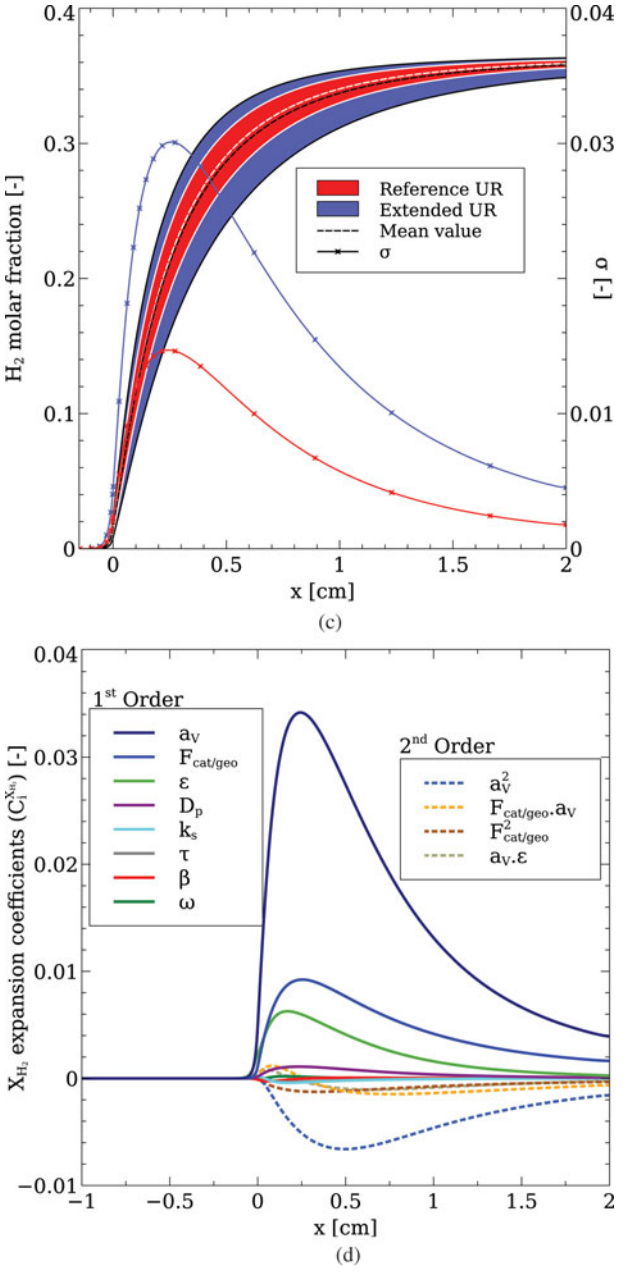

Figure 7. (*Continued*) (colour online)

that the S_{H_2} ensemble mean profiles increase as the distance from the catalyst inlet section increases due to an increase in the residence time that favours the progress of the slow reforming reactions. An exception is however noticed very near the catalyst entrance section ($x \leq 0.05$ cm) where the ensemble mean profiles slightly decrease. This can be attributed

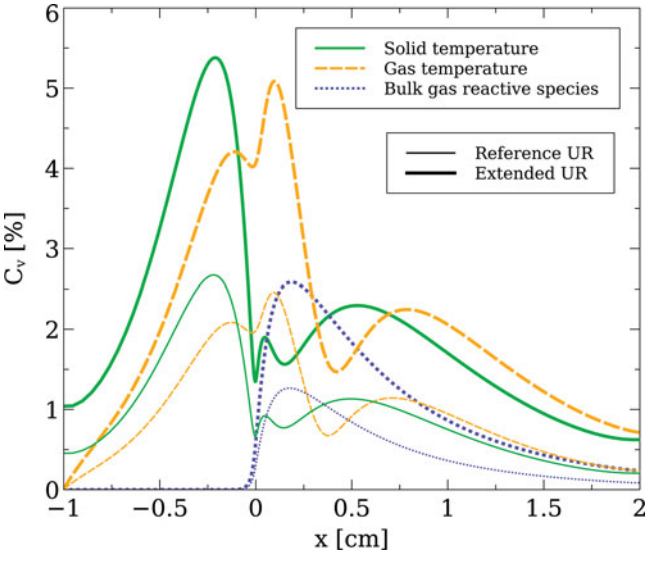

Figure 8. Coefficient of variation for the stochastic solution profiles of gas and solid temperatures and bulk gas reactive species composition. (colour online)

to an increase in the $\dot{\omega}_{H_2O}/\dot{\omega}_{H_2}$ ratio as Figure 4(a) suggests since the solid temperatures (ensemble mean profiles) increase up to near the section $x = 0.1$ cm following an overall promotion of the highly exothermic oxidation reactions that produce total oxidation species (H_2O and CO_2) instead of partial oxidation products (H_2 and CO). For both uncertainty ranges the uncertainty in the stochastic S_{H_2} solution profiles decreases from a maximum value located at $x \simeq 0.35$ cm towards the outlet section. As Figure 9(b) demonstrates, the uncertainty assigned to the model input parameters a_V, $F_{cat/geo}$ and ϵ is decisive in the stochastic solution profiles of S_{H_2}.

Regarding the carbon monoxide selectivity (Figure 9(c)) the ensemble mean profiles for the reference and extended URs present a maximum value within the catalyst bed (near the section $x = 0.4$ cm). The maximum value registered is due to a change in the ratio $\dot{\omega}_{CO_2}/\dot{\omega}_{CO}$: during the first millimetres of the catalyst bed ($x \leq 0.4$ cm) the net production rate of CO is higher than the net production rate of CO_2, while during the remaining catalyst length the converse tendency is verified. The uncertainty level of the S_{CO} stochastic solution profiles is generally much lower than the uncertainty level observed for the case of S_{H_2}. After attaining a minimum uncertainty level at $x = 0.62$ cm, the uncertainty in the S_{CO} stochastic solution profiles slightly increases along the remaining region of the catalyst bed reaching an uncertainty level comparable with the stochastic solution profiles of S_{H_2} ($c_V(S_{CO}) \simeq c_V(S_{H_2})$) near the outlet section. As before, regarding the S_{H_2} stochastic solution profiles, a_V, $F_{cat/geo}$ and ϵ are the key parameters in the total uncertainty level observed for S_{CO} (see Figure 9(d)).

The fuel conversion level can be an indicator of the approximation to thermodynamic equilibrium. Therefore, a value of 95% for methane conversion is chosen herein to identify the catalyst length required to achieve thermodynamic equilibrium conditions. Figure 10(a) shows the PDF of the reactor position where a fuel conversion equal to 95% is observed ($x\left(@X_{CH_4} = 95\%\right)$) for the reference UR. It is noticed that in the mean stochastic case a catalyst length of less than 1.0 cm is enough to attain such a fuel conversion level for the

operating condition and variability range employed. A difference of about 0.4 cm is found within the 95% CI envelope. It is concluded analysing Figure 10(b) that a_V, $F_{\text{cat/geo}}$ and ϵ are the input parameters with more impact on finding the reactor length required to achieve equilibrium conditions.

Since the momentum balance equation is not included in the mathematical model scheme the pressure drop along the whole reactor can be estimated in a post-processing stage of the deterministic solution with the Forchheimer equation considering the viscous and inertial permeability parameters from Incera Garrido et al. [30] as expression (22)

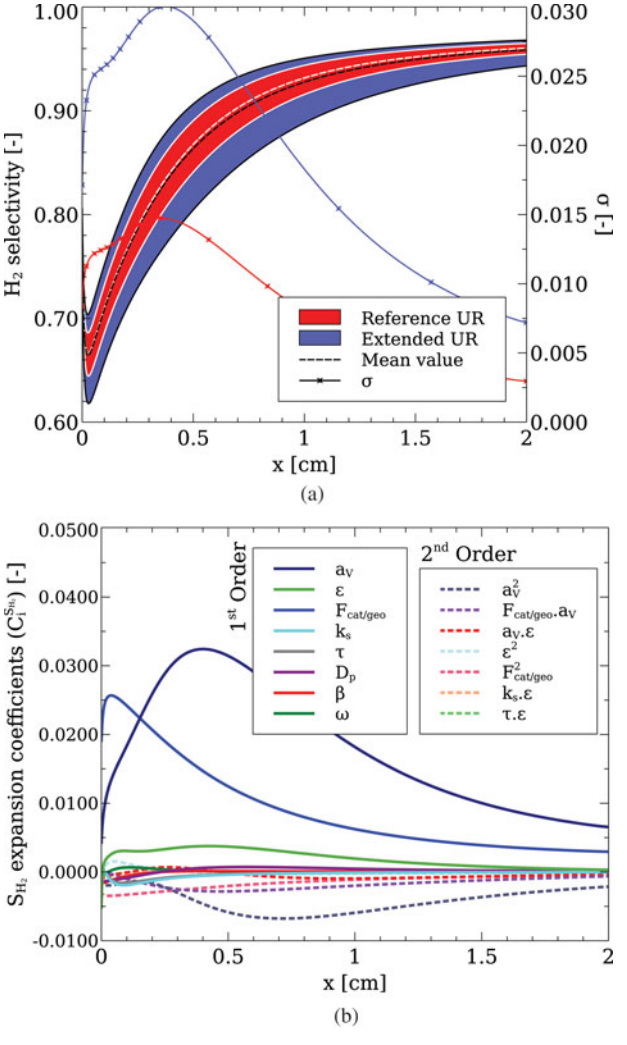

Figure 9. Stochastic solution profiles of bulk H_2 selectivity: (a) ensemble mean, standard deviation and error bars with 95% CI for the reference and extended URs; (b) most relevant expansion mode coefficients for the reference UR. Stochastic solution profiles of bulk CO selectivity: (c) ensemble mean, standard deviation and error bars with 95% CI for the reference and extended URs; (d) most relevant expansion mode coefficients for the reference UR. (colour online)

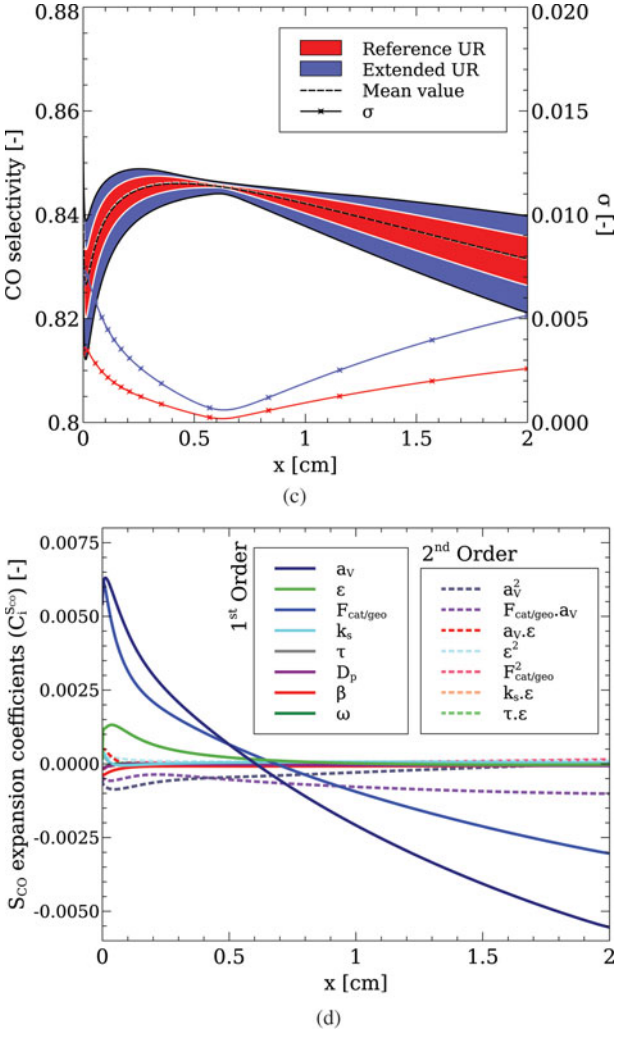

Figure 9. (*Continued*) (colour online)

shows:

$$\frac{\Delta P}{\Delta L} = \mu u \epsilon \left(1.42 \times 10^{-4} D_p[\mathrm{m}]^{1.18} \epsilon^{7.00}\right)^{-1} + \rho_g (u\epsilon)^2 \left(0.89 D_p[\mathrm{m}]^{0.77} \epsilon^{4.42}\right)^{-1}. \quad (22)$$

Figure 11(a) presents the PDF of the pressure drop in the whole reactor along with some statistics for the reference UR. A mean value for pressure drop around 3200 Pa is observed which is approximately 3% of the total pressure considered (atmospheric pressure) justifying the irrelevance of the pressure drop within the deterministic model formulation, even for the highly dense foams considered. A pressure drop difference of about 5000 Pa is noticed between the upper and bottom limits of the 95% CI envelope. Figure 11(b) reveals the contribution of each first-order coefficient as well as the main contributive

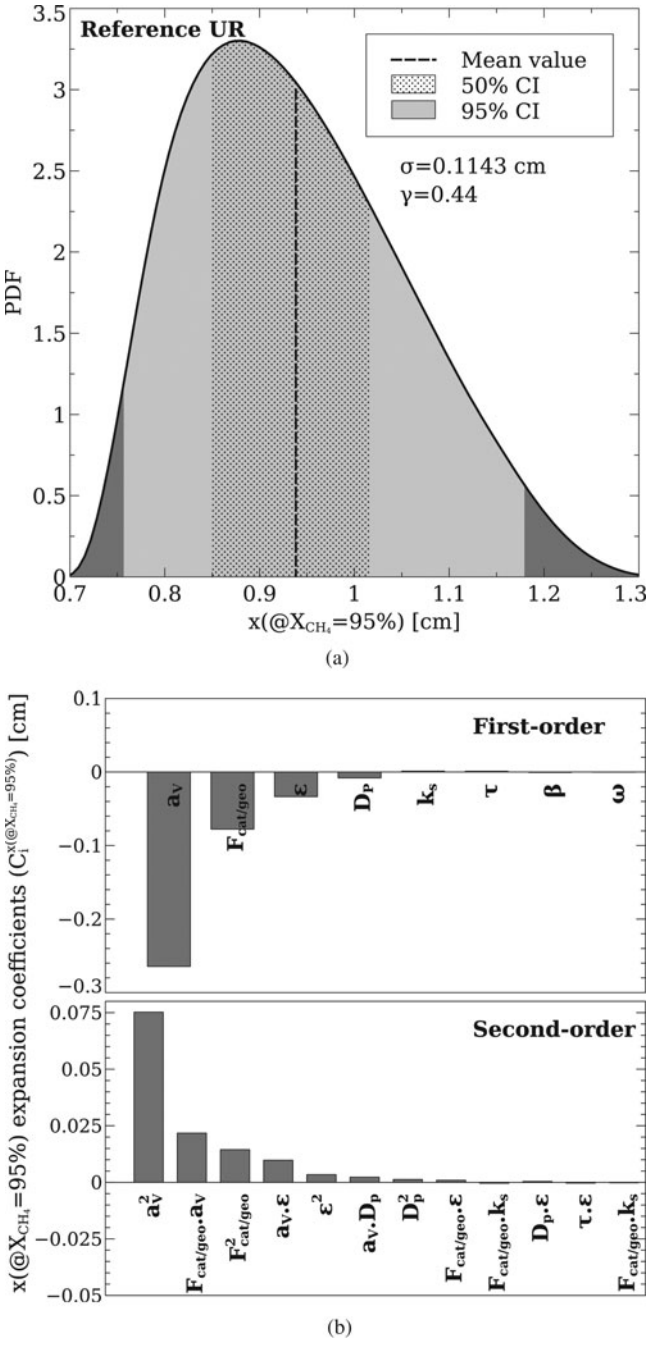

Figure 10. Stochastic solution of the axial reactor position where fuel conversion equals 95% for the reference UR: (a) PDF along with 50 and 95% CIs, ensemble mean value, standard deviation and skewness; (b) most relevant expansion mode coefficients. (colour online)

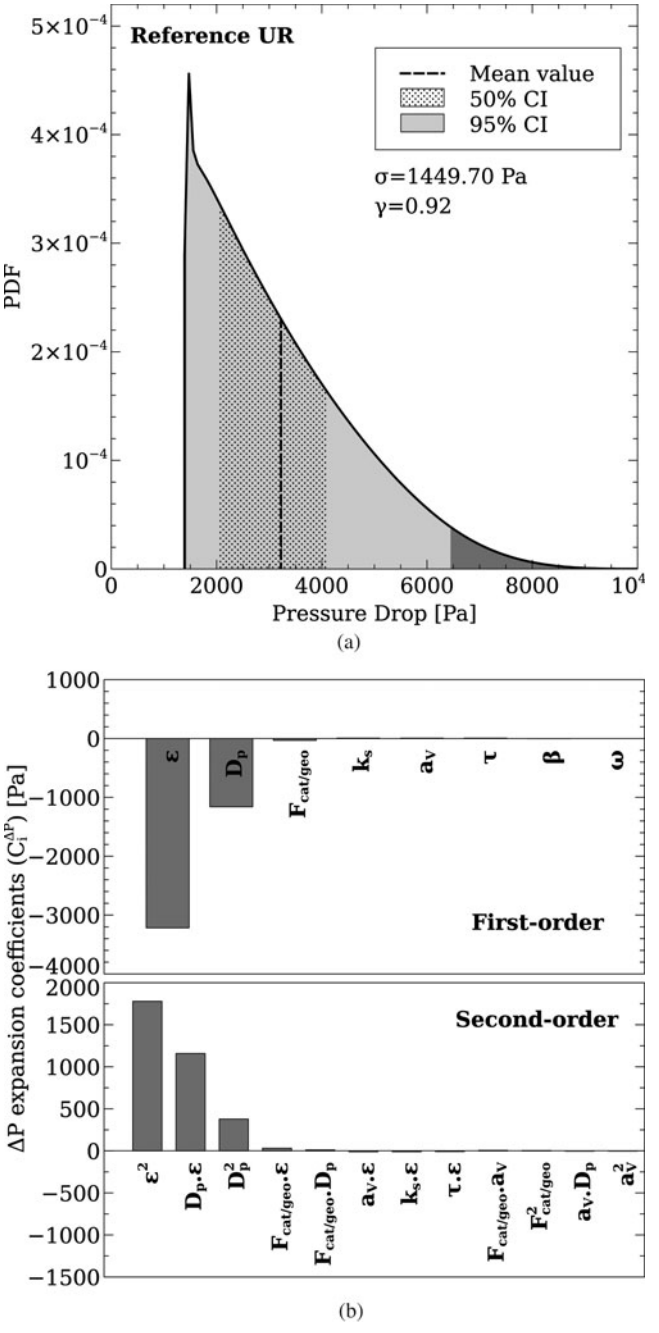

Figure 11. Stochastic solution of the pressure drop in the whole reactor for the reference UR: (a) PDF along with 50 and 95% CIs, ensemble mean value, standard deviation and skewness; (b) most relevant expansion mode coefficients. (colour online)

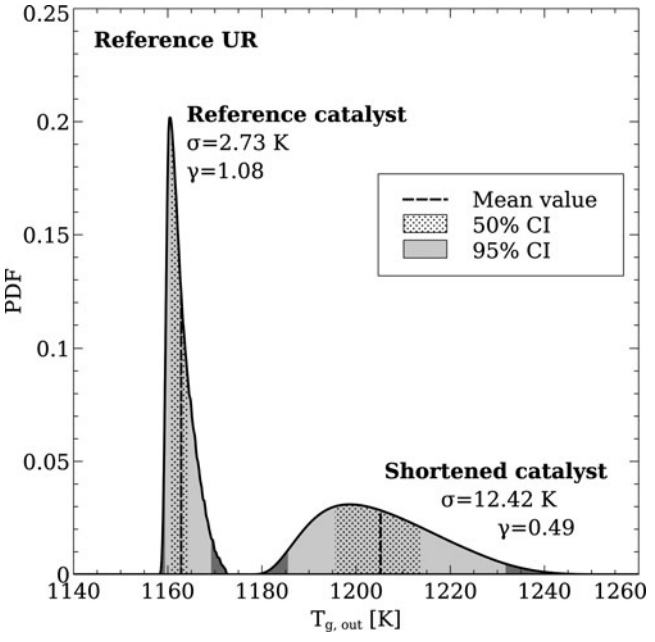

Figure 12. PDFs of the outlet reactor gas temperatures (reference UR) for the reference reactor geometry (reference catalyst) and for a reactor composed by a shortened catalyst with 1.0 cm in length (shortened catalyst). (colour online)

second-order coefficients. Porosity and pore diameter appear as the most important players in the pressure drop uncertainty due to their direct influence on expression (22). Other input uncertain parameters also induce an uncertainty due to their indirect impact on dynamic viscosity, density and superficial velocity profiles.

It was seen before that as the distance from the catalyst entrance increases the uncertainty in the stochastic temperature and species profiles tends to decrease and it becomes almost negligible near the catalyst outlet section. However, it should be noted that uncertainty traces in such variables at the outlet section will always be expected as long as the reactor operation is far from the adiabatic regime. If the modelling purpose is merely the evaluation of the outlet reactor conditions, then any uncertainty (even high) in the model input parameters would vanish in the outlet stochastic model solution for a long-enough and adiabatic catalyst. In such a situation, the outlet gas composition and temperature can be simply predicted by a chemical equilibrium calculation. In a practical case where a specific catalyst length and configuration are imposed, the impact of model input uncertainty on the outcome solution at the outlet catalyst section is not known *a priori*. In this case, the deterministic model solution computed with mean values can even indicate near the outlet section an approximation to thermodynamic equilibrium (by flat species and thermal profiles) which can cause a misleading interpretation of the impact of model input uncertainty on the stochastic solution because a relatively high level of uncertainty at the outlet section can always appear if the standard deviation of the input random parameters is high. Moreover, for a given reactor geometry and configuration the uncertainty level in the outlet solution variables is not only dependent on the applied variability ranges for the input random variables but also on the operating conditions (see [17]).

Figure 12 shows two PDFs for the outlet gas temperatures ($T_{\text{gas}}\,(x = 2.0\,\text{cm})$) considering the reference UR: the left PDF is for the present reactor configuration (Figure 1),

denoted the reference catalyst case, whereas the right PDF is for an equal reactor arrangement but with a shortened catalyst length ($L_{cat} = 1.0\,cm$) followed by a back heat shield ($L_{BHS} = 1.0\,cm$), denoted the shortened catalyst case. Regarding the discussion launched above about the influence of the catalyst length on the uncertainty level in reactor outlet solution variables, Figure 12 shows that the limits of the stochastic outlet gas temperatures (error bars) extend over a wider range in the shortened catalyst case than in the reference catalyst case. Although not presented, this finding is common to the remaining deterministic model dependent variables (surface temperature and species composition) at the outlet section for the shortened catalyst case with the current operating condition.

A final remark should concern the uncertainty due to the inlet boundary conditions, namely uncertainty in the gas phase balance equations due to an uncertainty in the feed mixture composition and temperature. It is expected that this kind of uncertainty would leave a significant mark, even for a long-enough and adiabatic catalyst (see [16]), contrary to what was observed previously for the eight input random parameters considered. This finds an explanation in the different chemical equilibrium states that are attained due to the different inlet mixture conditions. In the present work, the variables relating to the inlet mixture properties were considered without any uncertainty, mainly because it is not realistic to consider them random, as would be the case for a biogas feed mixture or for an anode off-gas from a fuel-cell in a post-combustion reactor. In the present case of methane CPOx, one should know the inlet gas composition and temperature.

4. Conclusions

The uncertainty of eight 1D model input random parameters in the catalytic partial oxidation of a methane–air mixture within a highly dense foam monolith reactor was quantified using the non-intrusive spectral projection approach based on polynomial chaos expansion. The selection of the input random variables and their variability is physically realistic.

It was observed regarding the stochastic temperature and mixture composition fields that uncertainty in the final solution varies along the axial (main flow) reactor direction. Among the random parameters that contributed most to the uncertainty observed in those variables are the porosity, the specific surface area and the ratio between catalytic and geometric surface area. Uncertainty in solid thermal conductivity and tortuosity led to a marginal impact on those variables. The mean pore diameter, although needed for the computation of external transport properties, did not play any important role in the final stochastic solution. Uncertainty in the mean pore diameter only appeared to be significant for the pressure drop along the whole monolith reactor. Regarding the uncertainty applied in the radiative heat transfer properties, even though high, no important effect of such uncertainty parameters was observed at all, even on the stochastic solid temperature profile.

It was noticed, for the operating condition and variability ranges considered, that the uncertainty in variables tends to become almost negligible at the outlet section due to the approximation to thermochemical equilibrium and because no uncertainty was prescribed for the inlet gas mixture composition and temperature. One can anticipate that the uncertainty assigned for the deterministic model input data vanishes from the outlet solution variables for a long-enough and adiabatic catalyst. However, most often for economic and practical reasons, catalysts are not so long for all operating conditions and variabilities applied on the input random parameters, and then stochastic models provide a useful insight regarding the expected ranges for the outlet solution variables.

Funding

This work was partially funded by the European Commission within the 7th Framework Program (CI-IP 260105 FC-DISTRICT).

References

[1] M.L. Perry, T.F. Fuller, *A historical perspective of fuel cell technology in the 20th century*, J. Electrochem. Soc. 149 (2002), pp. S59–S67.
[2] G. Groppi, A. Beretta, and E. Tronconi, *Monolithic catalysis for gas-phase syntheses of chemicals*, in *Structured Catalysts and Reactors*, A. Cybulski and J.A. Moulijn, eds., CRC Press, Boca Raton, 2006, pp. 243–310.
[3] D.A. Hickman, L.D. Schmidt, *Synthesis gas formation by direct oxidation of methane over Pt monoliths*, J. Catal. 138 (1992), 267–282.
[4] D.A. Hickman, E.A. Haupfear, L.D. Schmidt, *Synthesis gas formation by direct oxidation of methane over Rh monoliths*, Catal. Lett. 17 (1993), pp. 223–237.
[5] D. Dalle Nogare, N.J. Degenstein, R. Horn, P. Canu, L.D. Schmidt, *Modeling spatially resolved profiles of methane partial oxidation on a Rh foam catalyst with detailed chemistry*, J. Catal. 258 (2008), pp. 131–142.
[6] A. Beretta, G. Groppi, M. Lualdi, I. Tavazzi, P. Forzatti, *Experimental and modeling analysis of methane partial oxidation: transient and steady-state behaviour of Rh-coated honeycomb monoliths*, Ind. Eng. Chem. Res. 48 (2009), pp. 3825–3836.
[7] A. Donazzi, M. Maestri, B.C. Michael, A. Beretta, P. Forzatti, G. Groppi, E. Tronconi, L.D. Schmidt, D.G. Vlachos, *Microkinetic modeling of spatially resolved autothermal CH_4 catalytic partial oxidation experiments over Rh-coated foams*, J. Catal. 275 (2010), pp. 270–279.
[8] D. Scognamiglio, L. Russo, P.L. Maffettone, L. Salemme, M. Simeone, S. Crescitelli, *Modelling and simulation of a catalytic autothermal methane reformer with Rh catalyst*, Int. J. Hydrogen Energy 37 (2012), pp. 263–275.
[9] B.D. Phenix, J.L. Dinaro, M.A. Tatang, J.W. Tester, J.B. Howard, G.J. McRae, *Incorporation of parametric uncertainty into complex kinetic mechanisms: application of hydrogen oxidation in supercritical water*, Combust. Flame 112 (1998), pp. 132–146.
[10] H. Cheng, A. Sandu, *Efficient uncertainty quantification with the polynomial chaos method for stiff systems*, Math. Comput. Simulat. 79 (2009), pp. 3278–3295.
[11] M.T. Reagan, H.N. Najm, R.G. Ghanem, O.M. Knio, *Uncertainty quantification in reacting-flow simulations through non-intrusive spectral projection*, Combust. Flame 132 (2003), pp. 545–555.
[12] L. Mathelin, M.Y. Hussaini, T.A. Zhang, *Stochastic approaches to uncertainty quantification in CFD simulations*, Numer. Algorithms 38 (2005), pp. 209–236.
[13] D. Xiu, G.E. Karniadakis, *Modeling uncertainty in flow simulations via generalized polynomial chaos*, J. Comput. Phys. 187 (2003), pp. 137–167.
[14] M.T. Reagan, H.N. Najm, B.J. Debusschere, O.P. Le Maître, O.M. Knio, R.G. Ghanem, *Spectral stochastic uncertainty quantification in chemical systems*, Combust. Theory Model. 8 (2004), pp. 607–632.
[15] M. Dodson, G.T. Parks, *Robust aerodynamic design optimization using polynomial chaos*, J. Aircr. 46 (2009), pp. 635–646.
[16] M.A.A. Mendes, J.M.C. Pereira, J.C.F. Pereira, *Calculation of premixed combustion within inert porous media with model parametric uncertainty quantification*, Combust. Flame 158 (2011), pp. 466–476.
[17] M.A.A. Mendes, J.M.C. Pereira, and J.C.F. Pereira, *Parametric uncertainty quantification in modeling methane thermal partial oxidation within inert porous media*, in *Proceedings of the Vth European Conference on Computational Fluid Dynamics (ECCOMAS CFD)*, 14–17 June 2010, Lisbon, J.C.F. Pereira, A. Sequeira and J.M.C. Pereira, eds.
[18] M.S. Eldred, J. Burkardt, *Comparison of non-intrusive polynomial chaos and stochastic collocation methods for uncertainty quantification*, AIAA Paper 0976, 2009.
[19] M.A.A. Mendes, S. Ray, J.M.C. Pereira, J.C.F. Pereira, D. Trimis, *Quantification of uncertainty propagation due to input parameters for simple heat transfer problems*, Int. J. Therm. Sci. 60 (2012), pp. 94–105.

[20] O.P. Le Maître, O.M. Knio, H.N. Najm, R.G. Ghanem, *A stochastic projection method for fluid flow – I: Basic formulation*, J. Comput. Phys. 173 (2001), pp. 481–511.
[21] O.P. Le Maître, M.T. Reagan, H.N. Najm, R.G. Ghanem, O.M. Knio, *A stochastic projection method for fluid flow – II: Random process*, J. Comput. Phys. 181 (2002), pp. 9–44.
[22] H.N. Najm, *Uncertainty quantification and polynomial chaos techniques in computational fluid dynamics*, Annu. Rev. Fluid Mech. 41 (2009), pp. 35–52.
[23] J.C. Slaa, R.J. Berger, G.B. Marin, *Partial oxidation of methane to synthesis gas over* Rh/α–Al_2O_3 *at high temperatures*, Catal. Lett. 43 (1997), pp. 63–70.
[24] C.T. Goralski Jr, R.P. O'Connor, L.D. Schmidt, *Modeling homogeneous and heterogeneous chemistry in the production of syngas from methane*, Chem. Engng Sci. 55 (2000), pp. 1357–1370.
[25] A. Beretta, A. Donazzi, D. Livio, M. Maestri, G. Groppi, E. Tronconi, P. Forzatti, *Optimal design of a CH_4 CPO-reformer with honeycomb catalyst: combined effect of catalyst load and channel size on the surface temperature profile*, Catal. Today 171 (2011), pp. 79–83.
[26] S. Mazumder and M. Grimm, *Numerical investigation of radiation effects in monolithic catalytic combustion reactors*, Int. J. Chem. React. Eng. 9 (2011), pp. 1–18. Available at http://www.bepress.com/ijcre/vol9/A44.
[27] A. Schneider, J. Mantzaras, P. Jansohn, *Experimental and numerical investigation of the catalytic partial oxidation of CH_4/O_2 mixtures diluted with H_2O and CO_2 in a short contact time reactor*, Chem. Engng Sci. 61 (2006), pp. 4634–4649.
[28] S. Eriksson, A. Schneider, J. Mantzaras, M. Wolf, S. Järås, *Experimental and numerical investigation of supported rhodium catalysts for partial oxidation of methane in exhaust gas diluted reaction mixtures*, Chem. Eng. Sci. 62 (2007), pp. 3991–4011.
[29] B.T. Schädel, M. Duisberg, O. Deutschmann, *Steam reforming of methane, ethane, propane, butane, and natural gas over a rhodium-based catalyst*, Catal. Today 142 (2009), pp. 42–51.
[30] G. Incera Garrido, F.C. Patcas, S. Lang, B. Kraushaar-Czarnetzki, *Mass transfer and pressure drop in ceramic foams: a description for different pore sizes and porosities*, Chem. Engng Sci. 63 (2008), pp. 5202–5217.
[31] L. Kunz, L. Maier, S. Tischer, and O. Deutschmann, *Modeling the rate of heterogeneous reactions*, in *Modeling and Simulation of Heterogeneous Catalytic Reactions: From the Molecular Process to the Technical System*, O. Deutschmann, ed., Wiley-VCH, Weinheim, Germany, 2011, pp. 113–148.
[32] R.J. Kee, M.E. Coltrin, P. Glarborg, *Chemically reacting flow: theory and practice*, Wiley-Interscience, New Jersey, 2003.
[33] O. Deutschmann, R. Schwiedernoch, L.I. Maier, and D. Chatterjee, *Natural Gas Conversion in Monolithic Catalysts: Interactions of Chemical Reactions and Transport Phenomena*, Natural Gas Conversion VI, Studies in Surface Science and Catalysis 136, E. Iglesia, J.J. Spivey, and T.H. Fleisch, eds., Elsevier, 2001, pp. 251–258.
[34] M. Hartmann, L. Maier, H.D. Minh, O. Deutschmann, *Catalytic partial oxidation of iso-octane over rhodium catalysts: an experimental, modeling, and simulation study*, Combust. Flame 157 (2010), pp. 1771–1782.
[35] M.F. Modest, *Radiative Heat Transfer*, McGraw-Hill, New York, 1993.
[36] M.E. Larsen, J.R. Howell, *Least-squares smoothing of direct-exchange areas in zonal analysis*, J. Heat Trans. 108 (1986), pp. 239–242.
[37] M.H.N. Naraghi, B.T.F. Chung, *A unified matrix formulation for the zone method: a stochastic approach*, Int. J. Heat Mass Trans. 28 (1985), pp. 245–251.
[38] A.L. Boheman, *Radiation heat transfer in catalytic monoliths*, AIChE J. 44 (1998), pp. 2745–2755.
[39] S. Karagiannidis, J. Mantzaras, *Numerical investigation on the start-up of methane-fueled catalytic microreactors*, Combust. Flame 157 (2010), pp. 1400–1413.
[40] R.J. Kee, J.F. Grcar, M.D. Smooke, J.A. Miller, *PREMIX: a FORTRAN program for modeling steady laminar one-dimensional premixed flames*, SAND85-8240, Sandia National Laboratories, 1985.
[41] R.J. Kee, F.M. Rubley, E. Meeks, *CHEMKIN-II: a FORTRAN chemical kinetic package for the analysis of gas-phase chemical kinetics*, SAND89-8009, Sandia National Laboratories, 1989.
[42] R.J. Kee, G. Dixon-Lewis, J. Warnatz, M.E. Coltrin, J.A. Miller, *A FORTRAN computer code package for the evaluation of gas-phase multicomponent transport properties*, SAND86-8246, Sandia National Laboratories, 1986.

[43] G.P. Smith, D.M. Golden, M. Frenklach, N.W. Moriarty, B. Eiteneer, M. Goldenberg, C.T. Bowman, R.K. Hanson, S. Song, W.C. Gardiner Jr, V.V. Lissianski, and Z. Qin, *GRI-Mech 3.0*. Available at http://www.me.berkeley.edu/gri_mech/.

[44] D.G. Goodwin, *An open-source, extensible software suite for CVD process simulation*, in *Proceedings of CVD XVI and EuroCVD Fourteen*, 27 April–2 May 2003, Paris, M. D. Allendorf, F. Maury, and F. Teyssandier, eds., The Electrochemical Society, 2003, pp. 155–162.

[45] R.G. Munro, *Evaluated material properties for a sintered α-Alumina*, J. Am. Ceram. Soc. 80 (1997), pp. 1919–1928.

[46] D. Edouard, M. Lacroix, C.P. Huu, F. Luck, *Pressure drop modeling on solid foam: state-of-the-art correlation*, Chem. Eng. J. 144 (2008), pp. 299–311.

[47] J.G. Fourie, J.P. Du Plessis, *Effective and coupled thermal conductivities of isotropic open-cellular foams*, AIChE J. 50 (2004), pp. 547–556.

[48] X. Fu, R. Viskanta, J.P. Gore, *A model for the volumetric radiation characteristics of cellular ceramics*, Int. Comm. Heat Mass Trans. 24 (1997), pp. 1069–1082.

[49] J.E.P. Navalho, I. Frenzel, A. Loukou, J.M.C. Pereira, D. Trimis, J.C.F. Pereira, *Catalytic partial oxidation of methane rich mixtures in non-adiabatic monolith reactors*, Int. J. Hydrogen Energy 38 (2013), pp. 6989–7006.

[50] R. Horn, K.A. Williams, N.J. Degenstein, L.D. Schmidt, *Syngas by catalytic partial oxidation of methane on rhodium: mechanistic conclusions from spatially resolved measurements and numerial simulations*, J. Catal. 242 (2006), pp. 92–102.

[51] R. Horn, K.A. Williams, N.J. Degenstein, A. Bitsch-Larsen, D. Dalle Nogare, S.A. Tupy, L.D. Schmidt, *Methane catalytic partial oxidation on autothermal Rh and Pt foam catalysts: oxidation and reforming zones, transport effects, and approach to thermodynamic equilibrium*, J. Catal. 249 (2007), pp. 380–393.

[52] N.J. Degenstein, *Spatially resolved species and temperature profiles in the catalytic partial oxidation of methane and ethane*, Ph.D. diss., University of Minnesota, Minneapolis and St Paul, MN, 2007.